A Universal Method to Combat Multipaths for RFID Sensing

Ge Wang[†‡], Chen Qian[‡], Kaiyan Cui[†], Xiaofeng Shi[‡], Han Ding[†], Wei Xi[†], Jizhong Zhao[†], Jinsong Han[♯*]

[†]*Xi'an Jiaotong University, Xi'an, China.*
[‡] *University of California, Santa Cruz, CA, USA.*
[♯] *School of Cyber Science and Technology, Zhejiang University, China.*
[*] *Alibaba-Zhejiang University Joint Research Institute of Frontier Technologies, China.*

Abstract—**There have been increasing interests in exploring the sensing capabilities of RFID to enable numerous IoT applications, including object localization, trajectory tracking, and human behavior sensing. However, most existing methods rely on the signal measurement either in a low multipath environment, which is unlikely to exist in many practical situations, or with special devices, which increase the operating cost.**

This paper investigates the possibility of measuring 'multipath-free' signal information in multipath-prevalent environments simply using a commodity RFID reader. The proposed solution, Clean Physical Information Extraction (CPIX), is universal, accurate, and compatible to standard protocols and devices. CPIX improves RFID sensing quality with near zero cost – it requires no extra device. We implement CPIX and study two major RFID sensing applications: tag localization and human behavior sensing. CPIX reduces the localization error by 30% to 50% and achieves the MOST accurate localization by commodity readers compared to existing work. It also significantly improves the quality of human behaviour sensing.

Index Terms—**RFID, Sensing, Multipath, Localization**

I. INTRODUCTION

As a cost- and energy-efficient solution for the Internet of Things (IoT), Radio Frequency IDentification (RFID) technology has been widely used to connect tagged objects in ubiquitous applications, such as retailing, warehouse, transportation, and manufactures [13], [16]–[19]. Besides its basic tag-identification function, there has been a growing interest in recent research to discover the sensing capability of RFID tags that reflects the spatial-temporal information of the tags in the physical world [4], [36], [39]. Typical applications of RFID sensing include localization, trajectory tracking, human behavior sensing, *etc.*. The majority of these applications rely on the measurement of the received signal data from tags, including the *phase shift* between the reader to tags (we use "*phase*" hereafter) and the *received signal strength* (*RSS*).

For example, the phase measurement can help to derive the distance and angle of arrival (AoA) from the reader antennas to a tag and further localize the tag [2], [21]. A successive collection of the phases from a mobile tag can help to determine the moving trajectory of the tagged object [32], [33], [43], [46], [47]. Phases have also been used for human activity sensing [35], [43]. The RSS can also be used to infer the distance from a tag to the reader or the existence of a moving object around the tag. Hence there have been applications that localize the target tag [42] or detect human gestures [6], [8], [35] by observing the variation of the RSS.

For RFID sensing applications, accurate measurement of *the multipath-free physical information* of the backscatter signals is a must for their correct operations. The multipath-free physical information is defined as the phase and RSS of the signals without environment affection from a tag to the reader, which can reflect the actual distance and relative location changes. In this paper, we call the line-of-sight (LOS) signal phase as the *clean phase* and the RSS that is not affected by the environment as the *clean RSS*. Unfortunately, in most practical RFID setups, signals may be reflected by various reflectors in the environment [42], including walls, furniture, shelves, and moving persons. We consider these environments as *multipath-prevalent* environments. Multiple reflected signals combine with each other and result in measurement results extremely different from the clean ones. We provide an incomplete list of recent research about RFID sensing applications in Table I. We find that they **either cannot combat multipaths or require extra devices/restrictions**. They might assume low-multipath environments, no moving persons [21], [33], [46], or apply the following two approaches: 1) Collecting plenties of training data in the deployment area to estimate the multipath [31], [32], [47]. This type of methods only considers the static reflectors but obviously does not work when moving persons exist. 2) Using special hardware including Software Defined Radio (SDR) [5], [13], [23]–[26], [42], synchronised antenna array (*e.g.* MUSIC algorithm [30]), moving antennas [31], [42], robots [23], [31], [41], and broadband nonlinear backscatter devices [24]. These methods increase the device cost, may not be compatible with existing RFID systems, and only work for certain specific applications. We specify them in Sec. II.

This paper presents a low-cost, universal, and accurate solution of Clean Physical Information eXtraction (CPIX) in multipath prevalent environments. CPIX **achieves a significant quality gain of RFID sensing with little cost** – it requires no extra device or restriction in addition to the current operating RFID systems: reader, tags, and a data analysis server. Hence it is **a simple yet fundamental improvement** to a diverse group of RFID sensing applications.

We resolve a number of challenges in the design and implementation of CPIX, including the uncontrollable and

TABLE I
SOME RECENT RFID SENSING METHODS ("LOCALIZATION" MAY INCLUDE TRAJECTORY TRACKING)

Method	Task	Info. used	Combat multipath	Restrictions
RF-IDraw [43] *SIGCOMM*'14	Localization	Phase	✗	2 readers, 8 antennas, limited space
Tagoram [46] *MobiCom*'14	Localization	Phase	✗	N/A
BackPos [21] *Infocom*'14	Localization	Phase	✗	N/A
STPP [33] *NSDI*'15	Tag ordering	Phase	✗	Mobile antenna
Tagyro [45] *MobiCom*'16	Orientation	Phase	✗	N/A
APID [6] *UbiComp*'16	Behavior sensing	RSS	✗	N/A
RFIPad [7] *ICDCS*'17	Behavior sensing	Phase & RSS	✗	N/A
Tag-Compass [20] *Infocom*'17	Orientation	RSS	✗	N/A
RIO [29] *MobiCom*'17	Behavior sensing	Phase	✗	N/A
ReMix [38] *SIGCOMM*'18	In-body localization	Phase	✗	Non-commodity SDR-based equipments
PinIt [42] *SIGCOMM*'13	Localization	RSS	✓	SDR, mobile antenna, anchor tags
MobiTagbot [31] *MobiSys*'16	Tag ordering	Phase	✓	Mobile antennas, robot, training
BNB [24] *MobiCom*'16	Localization	Phase	✓	Non-commodity devices
RFly [25] *SIGCOMM*'17	Localization	Phase	✓	Drones and Non-commodity devices
RFind [26] *MobiCom*'17	Localization	Phase	✓	Non-commodity SDR-based reader
WiSh [13] *MobiSys*'18	Localization	Phase	✓	Non-commodity SDR-based reader
RF-Echo [5] *MobiCom*'17	Localization	Raw RF signals	✓	Non-commodity tags and reader
TurboTrack [23] *NSDI*'19	Localization	Raw RF signals	✓	Need an SDR-based reader and a complex localization Helper

unpredictable multipath reflections and device diversity. The basic idea of CPIX is to conduct signal measurement from multiple channels of a commodity reader. Our unique innovation is that we decompose the measured data into two parts: the contribution determined by the LOS signal and the contribution by the reflected signals, and then derive their mathematical relationships.

The state-of-the-art RFID systems can benefit from CPIX and obtain a much more accurate phase and signal strength measurement by simply installing the CPIX middleware program at a backend server connected to the reader. We thoroughly evaluate the effectiveness of CPIX by implementing it on two main-stream user applications, namely tag localization and human behavior sensing. For tag localization, we utilize the clean phases processed by CPIX as the input of a state-of-the-art hyperbola-based localization method [21]. The CPIX based localization algorithm can achieve median errors of 6.17~7.63cm (in different setups), which reduce the error of the hyperbola-based localization by 33% to 54% and is **the most accurate tag localization result by commodity devices**. The accuracy is also comparable to or higher than those in low-multipath lab environments by recent methods (some of them only apply to 2D) [21], [33], [46]. We also implement CPIX on a recent human behavior recognition application RFIPad [7] and find CPIX improves the accuracy of RFIPad by 10% to 20%. We demonstrate that CPIX is universally applicable to many sensing applications.

Our contributions are summarized as follows.

1) CPIX is the first generalized solution that can measure the multipath-free physical information by only COTS RFID devices. It is a middleware program running on the back server without extra hardware or hardware modification.

2) CPIX needs no deployment of reference/anchor tags or sensors, nor training data collection. It highly improves the application variety and convenience of CPIX.

3) We have done a thorough implementation and validate that CPIX significantly improves the accuracy of tag

localization and human behavior sensing. We believe CPIX could benefit a diverse group of RFID sensing applications.

The rest of paper is organized as follows. We review the related work in Section II. The model and validation of multipath reflections are presented in Section III. The system design and evaluation can be found in Section IV and V. Finally we conclude this paper in Section VI.

II. RELATED WORK

Tag localization and trajectory tracking: Due to the close relationship with the travel distance of signals, phases have been widely used in tag trajectory tracking and localization. BackPos [21] illustrates a specific method for tag localization by constructing a hyperbola with the received phases of the target tags, without using anchor tags. It can achieve a mean accuracy of $12.8cm$ with a variance of $3.8cm$. However, the accuracy of BackPos heavily relies on a low-multipath environment. MobiTagbot [31] is a recent method to determine the orders of a set of tags, which can work in multipath-prevalent environments. It needs extra hardware, i.e., a robot reader with mobile antennas, as well as extra training time. Besides localization, tag trajectory tracking has also been studied [27], [28], [38], [40], [43], [46], [49]. Tagoram [46] is designed to track a moving tag based on the hologram method using COTS RFID systems. RF-IDraw [43] requires a user to carry a tag on her finger and limit the movement within a small area. Then it can track the detailed trajectory shape of the moving tag with high accuracy. However, the performances of these work also rely on a low-multipath environment. RF-Echo [5], Broadband Nonlinear Backscatter [24], RFind [26] and TurboTrack [23] are recent localization methods that can combat the multipath effect. However, they both require extra hardware such as software-defined radio, non-commodity readers, antenna arrays and even self-defined tags.

Human behavior sensing: The movement of human body will interference the backscatter communication between the

RFID reader and tags. Researchers have studied the relationship between the received phase or signal strength profile and human activities [1], [3], [8], [12], [14], [29], [34], [35], [47], [48]. Tadar [47] introduces a device-free method for tracking moving objects through a wall. It can remove the influence of static objects, such as furniture, by collecting reference data in advance. RFIPad [7] is a human hand gesture detection system to recognize basic touchscreen operations and English letters. They all rely on low-multipath environments. In recent years, some researchers employ machine-learning tools and algorithms to explore and infer the human behavior among tremendous data in a multipath-prevalent environment. However, it needs considerable hardware costs, including additional antennas and computing support equipments, which limits its applications.

LOS identification techniques: Prior work in other technologies, such as WiFi and 60GHz wireless, may employ a frequency domain transform method to identify the line-of-sight signals [26]. The basic idea is to transform the frequency domain signals in a certain bandwidth into a time domain. Based on the fact that LOS signal arrives earliest in time, they choose the first peak as the estimation of the LOS signal. However, this method cannot be applied in COTS RFID system. That is because commercial RFID devices transmit RF signals at a certain central frequency and the bandwidth is extremely small (about 4MHz with InpinJ R420). Even though we can transform the frequency domain signals into the time domain, the LOS signal and other reflected signals will superpose with each other and cannot be distinguished. Besides frequency domain transformation, MUSIC is an algorithm used for finding the emitters' locations. Its basic idea is to estimate the direction of multiple arrived signals. However, this method needs a synchronous antenna array and corresponding supporting devices. However, the COTS RFID systems do not support the synchronous antenna array, even if it equipped with an antenna hub.

Multi-channel based signal measurement: The basic idea of CPIX to find out the internal relationship among the measurement of physical information from multiple channels of the reader and then infer the actual value of the clean phase/RSS. Multi-channel based signal measurement has been used in other technologies, such as WiFi, 60GHz wireless, and acoustic signals [37], [44]. However, RFID devices and protocols [9], [10] work differently from other wireless technologies and hence these methods cannot be applied directly to RFID.

III. BACKGROUND

Before we introduce our method, we first introduce the propagation model of the passive RFID system. A passive RFID tag communicates with the RFID reader by backscattering its electric signals. Since there are prevalent reflectors in the real world, the received signals at the reader's antenna can be expressed as a superposition of the line-of-sight (LOS)

(a) LOS and reflected signal   (b) Wave superposition
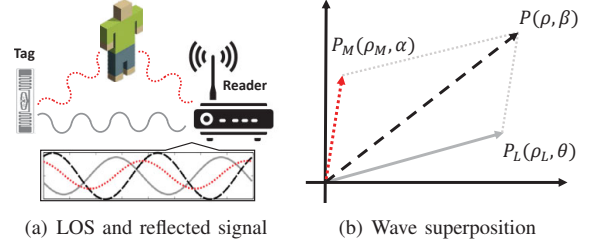
Fig. 1. RF signal propagation model. The two-dimensional coordinate system in (b) is a polar coordinate system, in which the vectors on this plane represent the RF signals.

signal P_L and the combined multipath signals P_M, *i.e.*:

$$P(\rho,\beta) = \underbrace{\rho_L \cdot \cos(2\pi f \cdot t_L + \theta)}_{LOS\ signal\ P_L} + \underbrace{\rho_M \cdot \cos(2\pi f \cdot t_M + \alpha)}_{Multipath\ signal\ P_M}$$
(1)

where f denotes the signal frequency, which can be considered as identical for both LOS and multipath signals. t_L and t_M are the signal transmitting time of LOS signal and multipath ones, respectively. β, θ and α represent the phases of the received signal, LOS signal and combined multipath signals respectively. And ρ, ρ_L and ρ_M are signals' amplitudes. The amplitude ρ can be estimated by the received signal strength (RSS), *i.e.*, $\rho = 10^{\frac{RSS}{1000}}$ [46]. Note that only the line-of-sight signal P_L has the following relationship with the distance between the reader and the tag [21], [46], [47]:

$$\theta = (\theta_A + \theta_T + \theta_D) \mod 2\pi$$
(2)

where θ_A and θ_T are the initial phases of the reader antenna and the tag, respectively. And θ_D is the corresponding phase change over the signal travel distance, which is defined as:

$$\theta_D = (2\pi \cdot 2d/\lambda) \mod 2\pi$$
(3)

where d is the distance from the antenna to the tag. $\lambda = c/f$ is the wavelength and c is the speed of electromagnetic signal. In contrast, the multipath signal P_M is determined by surrounding reflectors, such as moving objects like human beings, robots and static ones like furniture, walls, *etc.*. In addition, due to the non-negligible reflection attenuations, we have $\rho_M < \rho_L$.

A. Model of signal propagation

Observing the aforementioned elaborations, we find that the received signal P is not a linear relationship with the LOS signal P_L. As shown in Fig. 1, the received signal P (black dotted line) is the superposition of the LOS signal P_L (grey line) and current multipath signal P_M (red dotted line). However, we have no information about the multipath signal P_M. As a result, the COTS reader is not able to tell the LOS signal P_L from its received signal P. In other words, the physical data (including phase and RSS) we measured from the received signal cannot accurately reflect the exact values and changes of the LOS signal, causing existing work to be error-prone in multipath-prevalent environments. In the following subsection, we will verify the impact of the multipath effects with experiments.
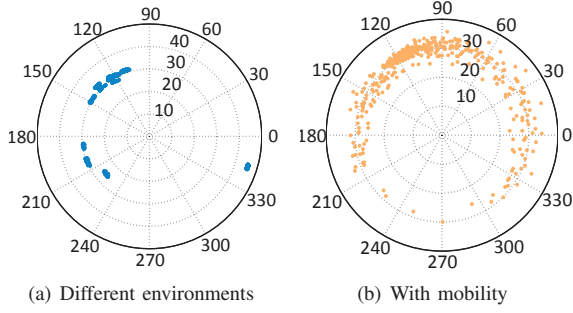
Fig. 2. Phase variations due to multipaths, radian is the phase and radius is the RSS (-dBm)

B. Experimental analysis of multipaths

We conduct two sets of experiments using COTS RFID devices to validate that multipath reflections will cause the measurement data (including phase and RSS) from the received signal completely unpredictable and deviated from the LOS ones. The first experiment is to show the ubiquity of multipath in different static environments. We place one tag in front of a reader, and then keep their separation distance unchanged, but move the whole system to 10 different locations in indoor environments. The received phases and RSSs of the same tag are shown in Fig. 2(a)[1],where the radius reflects the absolute value of RSS and the radian shows the degree of phase. We find that the phase measurement results have a huge variance in $(105°, 345°)$. This variance may introduce > 20cm errors when calculating the distance $([\lambda \cdot (345° - 105°)]/360° \approx 21$cm, for $\lambda \approx 32$cm), resulting in a destructive impact on tag localization and trajectory tracking. The second experiment is to investigate the signal fluctuations caused by moving objects. We let the reader keep querying a tag and collecting the signals for 10 seconds. During that time, a volunteer moves around the tag arbitrarily. As shown in Fig. 2(b), the values of phase are widely distributed in the 2π range and the RSS varies in [-30, -20]dBm. In other words, the movement of objects around the tag will make the phase and RSS measurements significantly different from the clean physical information and hence damage the performance of RFID sensing applications such as localization, human activity recognition, etc..

IV. CPIX DESIGN

The objective of CPIX is to extract the clean measurement information, namely the phase and RSS, from a tag in multipath environments. Extracting the multipath-free physical information from the measured data is challenging. **Our unique innovation is that we decompose the measured signals into two parts**: the contribution determined by the LOS signal and the contribution by the reflected signal, and derive their mathematical relationships. We further validate that measurement from different channels can be fitted with a linear function of the two types of contributions, which can be

---

[1]Whether the reader works with a fixed frequency or with hopping frequencies do not matter in our design.

used to extract the clean measurement. CPIX can be separated into three steps, including **1)** Phase decomposition. **2)** Clean phase calculation. **3)** RSS calculation. To be more clear, we list some key parameters used in our algorithm in Table. II.

A. Phase decomposition

As aforementioned, the received signal is a vector superposition of the LOS signal and other reflected ones. Therefore, in this step, we first explore the relationship between the LOS signal P_L and the received signals P.

We illustrate the relationship between the measured phase β and the clean phase θ, in Fig. 3. The radius of the vector represents the amplitude of the signal and the polar angle represents the current phase. As shown in Fig. 3(a), the gray line $\overrightarrow{OC}$ denotes the line-of-sight signal P_L, while the red line $\overrightarrow{OA}$ represents the superposition of all reflected signals, i.e., P_M. Their phases are θ and α, respectively. When $\overrightarrow{OC}$ and $\overrightarrow{OA}$ meet at the receiving antenna, they superpose with each other and form a new signal $\overrightarrow{OB}$, which is reported as the signal measurement, i.e., P.

We first build a bridge between the multipath signal and LOS signal. As shown in Fig. 3(a), we decompose the multipath vector $\overrightarrow{OA}$ into two parts, one vector $\overrightarrow{OA'}$ is perpendicular to LOS signal $\overrightarrow{OC}$, while another vector $\overrightarrow{OA''}$ is parallel to $\overrightarrow{OC}$. As shown in Fig. 3(b), we let $\overrightarrow{OC'} = \overrightarrow{OC} + \overrightarrow{OA''}$. The new polar angle α' of vector $\overrightarrow{OA'}$ has the following relationship with the former one:

$$\alpha' = (\theta + \frac{\pi}{2} + k_0 \cdot \pi) \ mod \ 2\pi \quad (4)$$

where k_0 is a non-negative integer. In the new forms, according to the Phasor arithmetic, we have a following equation:

$$\tan \beta = \frac{|\overrightarrow{OC'}| \cdot \sin \theta + |\overrightarrow{OA'}| \cdot \sin \alpha'}{|\overrightarrow{OC'}| \cdot \cos \theta + |\overrightarrow{OA'}| \cdot \cos \alpha'} \quad (5)$$

Considering the relationship between the values of α' and θ in Eq. 4, if we replace α' with θ in Eq. 5 we have:

$$\tan \beta = \frac{\tan \theta + (-1)^{k_0} \cdot \frac{|\overrightarrow{OC'}|}{|\overrightarrow{OA'}|}}{1 + (-1)^{k_0+1} \cdot \tan \theta \cdot \frac{|\overrightarrow{OC'}|}{|\overrightarrow{OA'}|}} \quad (6)$$

We find that θ and α' do not have a linear relationship with the phase β. In order to process them in a mathematical way, we define two *scalars*, $\hat{\theta}$ and $\hat{\alpha}$, whose sum is the received phase β, i.e.,

$$\beta = \hat{\theta} + \hat{\alpha} \quad (7)$$

where $\hat{\theta}$ is the contribution to β determined by θ and $\hat{\alpha}$ is the contribution to β determined by α. We call $\hat{\theta}$ as the *mirror image phases* of θ and $\hat{\alpha}$ as the *multipath variable*. According to the Trigonometric relation, we have:

$$\tan \beta = \tan(\hat{\theta} + \hat{\alpha}) = \frac{\tan \hat{\theta} + \tan \hat{\alpha}}{1 - \tan \hat{\theta} \cdot \tan \hat{\alpha}} \quad (8)$$

(a) Signals superposition   (b) Decompose signals
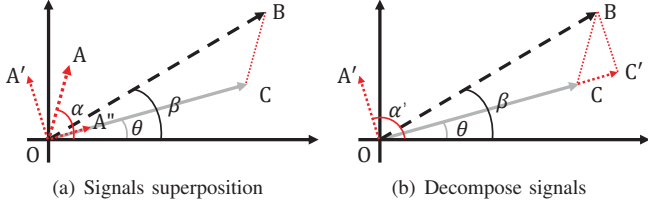
Fig. 3. Relationships between β and θ

Comparing Eq. 6 and Eq. 8, we find that the two variables, $\hat{\alpha}$ and $\hat{\theta}$, have the following relationship with θ:

$$\begin{cases} \hat{\theta} = (\theta + \hat{k} \cdot \pi) \bmod 2\pi, where \ \hat{k} \in Z \\ \hat{\alpha} = \arctan(-1)^{k_0} \cdot \dfrac{|\overrightarrow{OC'}|}{|\overrightarrow{OA'}|}, \end{cases} \quad (9)$$

In this way, we transform the measured phase β from the superposition of two unknown phases into a simple sum of two scalar phases $\hat{\alpha}$ and $\hat{\theta}$. In addition, we build a bridge between the desired clean phase θ and its image phase $\hat{\theta}$ (Eq. 9). In the following section, we will elaborate on how to calculate the value of the image phase $\hat{\theta}$ and finally infer the value of the clean phase θ.

B. Clean phase calculation

In the previous section, we find that the measured phase β does not have a linear relationship with the clean phase θ and multipath phase α. Instead, we choose two phases, namely the *multipath variable* $\hat{\alpha}$ and the *mirror image phase* $\hat{\theta}$, and build a linear equation with the measured phase β. In this section, we try to calculate the exact value of the *mirror image phase* $\hat{\theta}$ by exploring the internal relationship among the measured phases β in multiple channels.

We first introduce an observation and our conjecture about the received phase β in multiple channels. Recall that a reader has N channels ($N = 16$ in our experiments). We make a conjecture that the received phase β_n in channel n can be expressed as:

$$\beta_n = \hat{\alpha}_n + \hat{\theta} + (n-1) \cdot \Delta\hat{\theta} \quad (10)$$

where $\hat{\theta}$ refers to the mirror image phase in the first channel. $\hat{\alpha}_n$ is the *multipath variable* in channel n. Note that the *multipath variables* $\hat{\alpha}_n$ in channel n are *different* and *non-linear* for different channels[2]. On the contrary, the phase shift $\Delta\hat{\theta}$ between two adjacent channels is linear. It is composed of three parts, namely the phase changes $\Delta\theta_D$ over distance, phase changes $\Delta\theta_A$ and $\Delta\theta_T$ due to the device characteristics. When the channel is switched from n to $n+1$, the wavelength λ varies. As a result, the received signal over the same distance will incur a phase change of $\Delta\theta_D$. In addition, the initial

[2]The reasons are two-fold. First, signals' phases vary with the frequency, which means, even if the reflectors keep stable in the environment, the phases over the same reflection path are also different. Second, the path-loss and reflection attenuations are both different at different transmitting frequencies. The theoretical path loss in free space [11], [15], [50] is $FSPL(dB) = 20log_{10}(d) + 20log_{10}(f) - 27.55$. And the reflection attenuation in free space can be denoted as $RL(dB) = 20log\frac{Z_{in} - Z_0}{Z_{in} + Z_0}$, where Z_{in} is the impedance, which is related to the frequency. As a result, the multipath variables $\hat{\alpha}_n$ of different channels will be not only inconformity, but also non-linear.

(a) The reported phases   (b) The fitting line
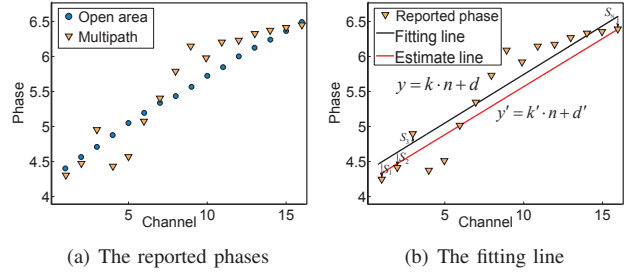
Fig. 4. The reported phases in 16 channels

phases of the antenna and tag will change by $\Delta\theta_A$ and $\Delta\theta_T$, respectively. Observing the three components of $\Delta\hat{\theta}$, we find that all of them are introduced by frequency hopping. As the frequency varies linearly among different channels, the phase shift $\Delta\hat{\theta}$ should be linear as well.

To validate the aforementioned conjecture, we perform a set of experiments. We place a tag in two different places, *i.e.*, an open area and a multipath-prevalent environment, and record the reported phases β_n in each channel. The results are shown in Fig. 4(a). The measurement phases in the open area are roughly on a straight line y'. That is because the effect of multipath signals in the open area is negligible when it is compared with the line-of-sight one, *i.e.*, $\hat{\alpha}_n \ll \Delta\hat{\theta}$. Hence we can safely express the straight line y' as:

$$y' = \kappa' \cdot n + d', where \ \kappa' = \Delta\hat{\theta}, d' = \hat{\theta} - \Delta\hat{\theta} \quad (11)$$

We call y' as the ideal line, which is only correct when there is no multipath effect. According to Fig. 4(a), the reported phases in the open area (the blue dots) indeed follow the linear relationship, which is consistent with our conjecture. On the other hand, in a narrow space, the multipath effect becomes severe. In the second experiment, the multipath variables $\hat{\alpha}_n$ cannot be ignored. As a result, the phase fluctuates sharply from channel 1 to 16, as outlined by the orange triangles in Fig.4(a).

In fact, the measured data in practice is more likely to be inaccurate and error-prone. To retrieve the exact value of tag's mirror image phase $\hat{\theta}$ from the measured one, *i.e.*, β, we analogize the Eq. 10 as a matrix equation $A \cdot x = b$, *i.e.*,

$$A_{N \times (N+2)} = \begin{bmatrix} 1 & 0 & 0 & ... & 0 & 1 & 0 \\ 0 & 1 & 0 & ... & 0 & 1 & 1 \\ 0 & 0 & 1 & ... & 0 & 1 & 2 \\ . & . & . & . & . & . & . \\ . & . & . & . & . & . & . \\ . & . & . & . & . & . & . \\ 0 & 0 & 0 & ... & 1 & 1 & N-1 \end{bmatrix}, \quad (12)$$

$x_{N+2 \times 1}^T = [\hat{\alpha}_1, \hat{\alpha}_2, \hat{\alpha}_3, ... \hat{\alpha}_N, \hat{\theta}, \Delta\hat{\theta}],$
$b_{N \times 1}^T = [\beta_1, \beta_2, \beta_3, ... \beta_N],$

where $A_{N \times (N+2)}$ is the coefficients matrix, $x_{(N+2) \times 1}$ is the unknown variable matrix, and $b_{N \times 1}$ represents the matrix of reported phases. And $(\cdot)^T$ represents the transpose of the matrix. Obviously, Eq. 12 is a set of non-homogeneous linear equations. Since we have $N + 2$ unknown variables and N equations, the solution of x has infinite possible candidates.

TABLE II
THE KEY PARAMETERS

Para.	Expression	Para.	Expression	Para.	Expression
θ	The phase of the LOS signal.	β, β_n	The received phase (in channel n).	α	The phase of the multipath signals.
$\hat{\theta}$	The mirror-image of θ.	$\hat{\alpha}, \hat{\alpha_n}$	The multipath variable (in channel n).	$\Delta\hat{\theta}$	The phase between two adjacent channels.
y'	The ideal line.	κ', d'	The slope and the intercept of the ideal line.	ω_n	The weight of the data in channel n.
y	The fitting line.	κ, d	The slope and the intercept of the fitting line.	y_n	The value on the fitting line at channel n.
φ	The optimization function.	e_1, e_2	The errors introduced by multipath effects.	S_n	The residual error at channel n.

To find out the valid solution of x, we need to establish two more additional equations.

To achieve this goal, we fit these reported phases β_n in all channels into a line. We define the fitting line as $y_n = \kappa \cdot n + d$, which has the minimal φ as follows:

$$\varphi = \sum_{n=1}^{N} \omega_n \cdot (y_n - \beta_n)^2, \tag{13}$$

where ω_n is the weight of channel n. Intuitively, the multipath effects are not identical for each channel. We define a weight function to reduce the influence of severe influences of outliers. The principle to determine the weight function is very simple, *i.e.*, a more serious *dynamic* multipath effect leads to more discrete phase reports. As we know, the dynamic reflectors, such as moving objects and humans, will introduce the uncontrollable and unpredictable errors into the measured phases. In contrast, the *static* multipath effect, which introduced by static objects like walls, ceilings, and furniture, will be much more stable and have a normal distribution [19]. Our goal is to reduce the influence of dynamic multipath, and try to estimate the exact effects of static multipath signals. Therefore, we divide the $\hat{\alpha}_n$ into two parts, $\hat{\alpha}_n = \hat{\alpha}_n^s + \hat{\alpha}_n^d$, where $\hat{\alpha}_n^s$ represents the contribution of static reflectors, and $\hat{\alpha}_n^d$ comprises of the impact introduced by moving objects. We utilize the sample mean difference σ_n of received phases in channel n to represent the discrete degrees: $\sigma_n = \frac{\sum |\beta_n^0 - \overline{\beta_n}|}{t}$, where β_n^0 represents the reported phase samples in channel n, and $\overline{\beta_n}$ is the average value of all the t samples. We further define the weight function as:

$$\omega_n = \frac{N \cdot p_n}{\sum p_n}, n = 1, 2, 3...N, \tag{14}$$

Here we define $p_n = e^{(\sum_{n=1}^{N} \sigma_n) - (N \cdot \sigma_n)}$. The p_n measures the discrete level of the n-th channel among all the N channels [31]. To make the weighted function easy to solve, we further process the measurement p_n with Eq. 14. The sum of all ω_n equals to the number of channels, *i.e.*, N. In this way, we reduce the weights of severely polluted channels in order to eliminate the impact of the uncontrollable and dynamic multipath effect. Since the dynamic multipath effects follow a Gaussian distribution[3], when the sample number t is sufficiently large, we can safely make an assumption that $\sum_{n=1}^{N} \omega_n \cdot \hat{\alpha}_n^d \approx 0$. The weight function will help us to find a more appropriate fitting line and ultimately, to get accurate results.

[3]The experiments and explanations can be found in [19].

Determining the most appropriate values of rake ratio κ and intercept d for the fitting line requires minimizing φ in Eq. 13. To achieve this goal, we calculate the partial derivative of φ for variable κ and d, respectively:

$$\begin{cases} \frac{\partial \varphi}{\partial \kappa} = \sum_{n=1}^{N} \omega_n \cdot [2n^2 \kappa + 2n(d - \beta_n)] \\ \frac{\partial \varphi}{\partial d} = \sum_{n=1}^{N} \omega_n \cdot [2d + 2(\kappa \cdot n - \beta_n)] \end{cases} \tag{15}$$

Let Eq. 15 equals 0 and solve the equations. We have:

$$\begin{cases} \kappa = \Delta\hat{\theta} + e_1, \ e_1 = \frac{N \cdot \sum \omega \cdot n \cdot \hat{\alpha}_n - \sum \omega \cdot n \cdot \sum \omega \cdot \hat{\alpha}_n}{N \cdot \sum \omega \cdot n^2 - (\sum \omega \cdot n)^2} \\ d = \hat{\theta} - \Delta\hat{\theta} + e_2, \ e_2 = \frac{\sum \omega \cdot n^2 \cdot \sum \omega \cdot \hat{\alpha}_n - \sum \omega \cdot n \cdot \hat{\alpha}_n \cdot \sum \omega \cdot n}{N \cdot \sum \omega \cdot n^2 - (\sum \omega \cdot n)^2} \end{cases} \tag{16}$$

We find that the slope κ and the intercept d of the fitting line y have an error e_1 and e_2 with that of the ideal line, respectively. If we can make sure the value of the errors, we can estimate the value of our expected value, $\hat{\theta}$. To do so, we find two additional equations:

Equation I: Intuitively, the first equation we built is one of the equations in Eq. 16:

$$\kappa = \Delta\hat{\theta} + e_1 \tag{17}$$

Note that another equation in Eq. 16 has the same effect as Eq. 17. We can utilize either of them.

Equation II: As shown in Fig. 4(b), the points y_n on the fitting line have a gap with the reported phase β_n. We define the difference between each pair of y_n and β_n as *residual error S_n*, *i.e.*:

$$S_n = y_n - \beta_n, n = 1, 2, 3...N \tag{18}$$

According to the Eq. 16, the residual error S_n can be transformed into another expression, *i.e.*, the second desired equation:

$$S_n = n \cdot e_1 + e_2 - \hat{\alpha}_n, n = 1, 2, 3...N \tag{19}$$

With Equ. 17 and 19, we can solve all the unknown variables in matrix x, including the mirror image phase $\hat{\theta}$ and the multipath variable $\hat{\alpha}$. Since $\hat{\theta} = (\theta + \hat{k} \cdot \pi) \mod 2\pi$ (Eq. 9), the clean phase θ has two feasible solutions. However, the value of clean phase θ is limited by the received phase β: $\angle BOC' = (\theta - \beta) \mod 2\pi < \frac{\pi}{2}$. Hence we can determine the solution of θ that meets such a requirement. Due to space limit, we skip the details.

C. RSS calculation

Besides phases, the measured RSS profile is not reliable as well. We conduct an experiment to explain it. We ask a volunteer to push her right hand in a crowded lab, and use a

(a) Deapth figure   (b) Movement path   (c) The profiles of RSS w/o CPIX
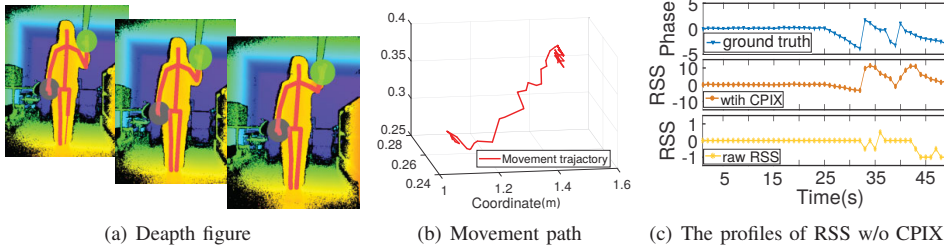
Fig. 5. A volunteer pushes the right hand and the ground truth can be obtained by Kinect

Fig. 6. Model of the signals

Kinect to capture the movement trajectory (as shown in Fig. 5). According to the movement trajectory obtained by the Kinect, we further calculate the phase profile of this activity (as shown in the top figure in Fig. 5(c)). Obviously, the received RSS can not accurately reflect the tendency of the movement (as shown in the bottom figure in Fig. 5(c)).

Our basic idea towards this problem is utilizing the geometrical relationship between the former received signal $\overrightarrow{OB}$ and the later one, $\overrightarrow{OB'}$, to infer the human interference signal $\overrightarrow{OD}$. Consider an example in Fig. 6, $\overrightarrow{OB}$ is the received signal at the reader. At that time, a human movement introduces a new multipath signal, *i.e.*, $\overrightarrow{OD}$ in Fig. 6. Then the current received signal changes to $\overrightarrow{OB'}$. Our goal is to retrieve the amplitude of $\overrightarrow{OD}$ at each time point and to estimate the behavior RSS. In fact, the information (including the amplitudes and phases) of the received signals $\overrightarrow{OB}$ and $\overrightarrow{OB'}$ can be directly obtained with commercial readers. According to Edge and Side axioms (SAS) [22], we can further make sure the remaining edge, $\overrightarrow{BB'}$, which is a translational vector of $\overrightarrow{OD}$. $\overrightarrow{BB'}$ has the same length and orientation with the vector $\overrightarrow{OD}$. In this way, we estimate the amplitude of $\overrightarrow{OD}$ by solving the aforementioned triangle problem.

The RSS profile estimated by CPIX and the one originally collected by the reader are also exhibited in Fig. 5(c). We find that the RSS profile estimated by CPIX is very similar to the ground truth, while the raw RSS signal is not.

V. EVALUATION AND CASE STUDY

To thoroughly evaluate CPIX, we implement CPIX on COTS RFID devices and apply it to two mainstream RFID sensing applications, including tag localization and human behavior sensing. We evaluate the performance of the two applications and compare them to the methods without CPIX.

A. Prototype implementation

Hardware: the CPIX prototype includes **nothing more than the basic components** of a typical passive RFID system: an RFID reader, several directional antennas, a set of tags, and a backend server, which are all commodity devices. In specific, we use an ImpinJ Speedway R420 RFID reader, four Laird S9028PCL directional antennas, and four types of mainstream UHF passive RFID tags: ImpinJ E41C, E41B and Alien 9710, Alien 9640. Note it is usual for a reader to carry multiple antennas to improve the coverage, and the price of an antenna is much cheaper than the reader. The R420 reader operates at the UHF frequency band (920.625 ∼ 924.375 MHz) and is able to hop over 16 channels. The gaps between two adjacent channels are the same, *i.e.*, 0.25 MHZ. The inventory mode is FM0, which can support about 380 successful queries per second. Each directional antenna has a gain of 8dBi and a size of 25cm×25cm. We run the software components of CPIX at a Dell desktop, which equips Intel Core i7-7700 CPU at 3.6 GHz and 16G memory. The ground truth data are obtained by laser range finder and Kinect, which are not required by CPIX.
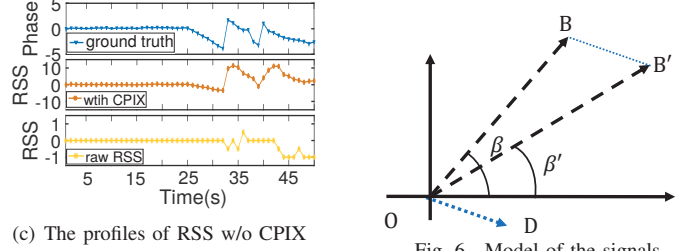
Software: The backscatter communication of RFID uses two mainstream protocols, namely LLRP [10] and EPC Class 1 Generation 2 (C1G2) [9]. The reader communicates with passive tags according to EPC C1G2, and the reader reports the information back to the server based on LLRP. The CPIX software on the PC is implemented using $C^\#$.

B. Use case 1: Tag localization

Localization is the most commonly proposed RFID sensing application. It is also the basis of another important application, trajectory tracking. To emulate the practical environments, we conduct experiments in three different environments, *i.e.*, the "*hallway*" (HW), "*laboratory*" (Lab), and "*Office*" (OF), as shown in Fig. 7. In the three environments, multipath reflections exist and could be a critical factor that impacts the localization accuracy. Intuitively, the laboratory environment is considered to include more multipath reflectors than the hallway. Besides walls and grounds, many furniture like cabinet may be a strong reflector. While the office may contain even more multipath sources than the laboratory. The tagged items are placed among a mess of metal products like computer and screen, plastics, glasses and textile fabrics. **The Office environment is more complex than most environments used in existing work listed in Tables I.**

We deploy 80 passive RFID tags in all. Among them, 12 are ImpinJ E41C tags, 40 are ImpinJ E41B tags, 20 are ALN-9710 and the other 8 are ALN-9640 tags, for the reader to localize. We utilize four antennas and form them as a square (as shown in Fig. 7). The coordinate origin of the deployment space is set as the center of this square. The tags we try to localize are at different positions. Their location varies among -82cm∼16cm in height (z-axis), -89cm∼104cm in width (y-axis), and 92cm∼300cm in depth (x-axis). For the hallway experiments, in each round, only one tag is interrogated and the multipath effect is much weaker than that of the laboratory and office environment. While for laboratory/office environments, we place 20/10 tags in the area and localize all

(a) Hallway (HW) (b) Laboratory (Lab) (c) Office (OF) (d) Results in Office (e) In a box
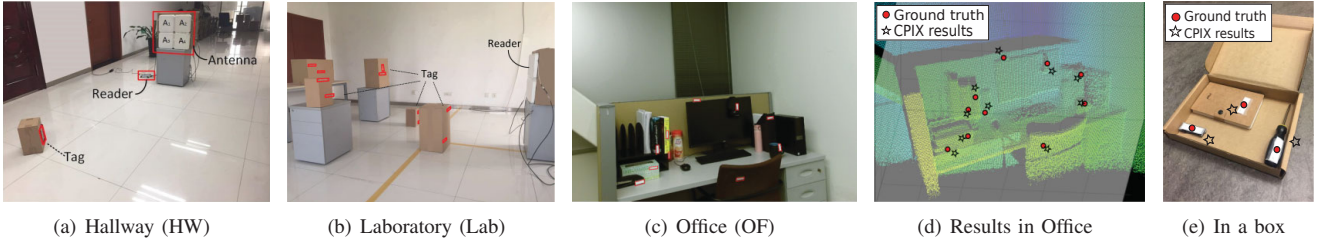
Fig. 7. Experiment environments and localization results of CPIX

(a) No mobility (b) With mobility

Fig. 8. Mean localization errors

Fig. 9. Distance vs. Error

Fig. 10. Sample number vs. Error
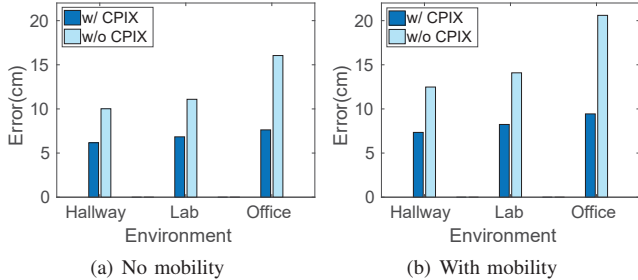
of them at the same time. For each environment, we conduct two sets of experiments. One is without moving objects and another has one volunteer keep walking arbitrarily in the area. The walking speed is 1∼2m/s. We call these two setups as "*no mobility*" and "*with mobility*".

The localization algorithm is a recently developed Hyperbola-based Localization (HL) method introduced in [21], [43]. We do not change the existing localization algorithm and just feed the algorithm with two sets of phase data, because our objective is to evaluate the quality of the phase data reported by CPIX rather than a new localization method.

Localization errors. In Fig. 8, we show the mean localization errors of the HL algorithm when using the CPIX phase (w/ CPIX) and the phase data from the reader API (w/o CPIX) respectively. We find that CPIX evidently reduces the HL errors in all environments, with and without mobility. The error reduction rate in Hallway is 38.4% (10.02cm to 6.17cm) without mobility and 41.2% (12.48cm to 7.34cm) with mobility. The error reduction rate in Lab is 32.7% (11.09cm to 7.58cm) without mobility and 41.5% (14.09cm to 8.24cm) with mobility. The error reduction rate in Office is 52.5% (16.05cm to 7.63cm) without mobility and 54.2% (20.6cm to 9.43cm) with mobility. We find when the environment is more complex and includes mobility, the multipath are more significant and the error reduction using CPIX is more obvious.

We also test the ability of CPIX on penetrating obstacles. We put the tagged things in a paper box, and then close the box and try to localize the tags inside the box. The estimation results of CPIX are shown in Fig. 7(e). We find that though the box blocks the LOS signals and introduce more reflections, the localization errors are still acceptable in this case. In this case, CPIX shows **possibilities of localizing none-line-of-sight objects** with a COTS reader.

Distance versus error. We also investigate the relationship between localization error and tag distance to the antennas in the lab environment. We place 40 tags in 4 different distances: 0.5m, 1m, 2m, and 3m, each with 10 tags. The
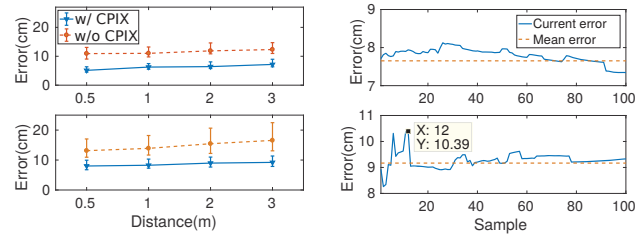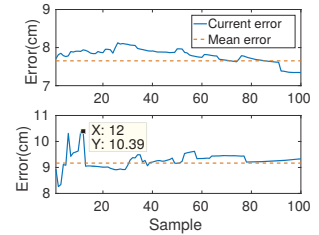
distance from the tag to the reader varies evenly in 0.5m to 3m. According to Fig. 9, the mean error by utilizing CPIX for 0.5m, 1m, 2m and 3m are 5.13cm, 6.26cm, 6.42cm and 7.18cm, respectively, which is much better than the original HL method (10.95cm, 11.01cm, 11.87cm, 12.32cm). In addition, CPIX works well even with one person moving around (8.01cm, 8.27cm, 8.98cm, 9.22cm). CPIX can achieve a good localization accuracy even when the distance is 3m, which is considered to be far in most existing work.

Number of samples versus error. In our experiments, an RFID reader stays at each channel for a short time period. During this period, the reader is able to collect a number of samples of tag replies. We expect to use fewer samples yet achieve higher localization accuracy. We then observe the relationship between the number of samples and the localization error. In Fig. 10, we show the error in the office environment when utilizing the first M samples ($M = 1, 2, ...100$). The top figure shows the errors in 'no mobility' case, while the bottom one shows the results with mobility. We find that the errors are stable without mobility, and vary from 7.34cm to 8.13cm. While for dynamic case, the errors fluctuate sharply before the first 12 samples, and quickly converge to the mean error. Note that in UHF passive RFID systems, the throughput of inventorying tags is very high. Normally a tag can report up to 380 samples to the reader per second. Hence CPIX only requires a trivial time for collecting phase data while providing a high localization accuracy.

Number of channels versus error. In CPIX, we may use up to all 16 channels. It is worth to investigate the minimum number of channels required for this method, considering that in some extreme applications the time duration for localizing a tag may be limited to allow a reader to traverse only a small number of channels. We then alter the number of channels from 3 to 16 involved in each experiment and show the results in Fig. 11. The left figure shows the results without moving person. We find that the mean error reduces slowly when the number of channels increases. Using only three channels

(a) No mobility   (b) With mobility
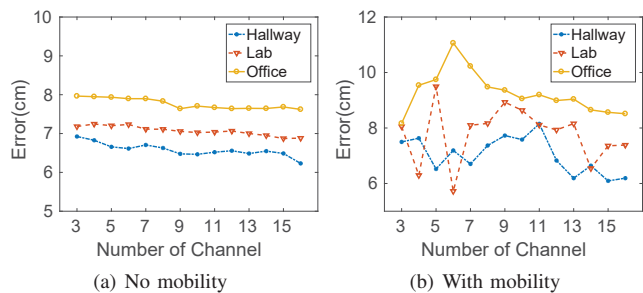
Fig. 11. Channel number vs. Error

TABLE III
THE SIMILARITY OF GROUND TRUTH SIGNAL AND THE SIGNALS
WITH/WITHOUT CPIX.

Method	RSS	Phase
Raw data	30.18%	72.66%
with CPIX	89.26%	82.17%

Fig. 12. Experiment deployment

(a) '⟶'   (b) '↓'

(c) '↘'   (d) '⊙'

Fig. 13. Five hand trajectories of four strokes

TABLE IV
ACCURACY OF RFIPAD WITH/WITHOUT CPIX

Data	CPIX	⟶	↓	↘	⊙
RSS	w/o	60%	73.33%	80%	73.33 %
	w/	80%	86.67%	86.67%	93.33%
Phase	w/o	73.33%	86.67%	80 %	86.67%
	w/	80%	93.33%	86.67%	93.33%

could achieve a mean localization error <7cm. While the right one shows error variations with a person moving around. The errors fluctuate among channels. However, the error in the worst case is no larger than 8.15cm/9.49cm/11.06cm in HW/Lab/OF environments.

C. Use case 2: Human activity sensing

To evaluate the performance of CPIX on combating multi-path effects in human activity sensing, we conduct two sets of experiments. The first is validating CPIX on accurately retrieving human activities. The second one is applying CPIX to an existing activity sensing system, RFIPad [7].

Accurately retrieving the human activity. In this set of experiments, we ask two volunteers to perform three activities, namely pushing hands, pulling hands and raising legs. To evaluate the performance of CPIX on coping with multipath effects, we conduct the experiments in three different places. At all these places, the volunteer is surrounded by many strong reflectors, including several metal cabinets, tables, and other furniture. We use a Kinect to capture the ground truth of the movement paths of the activity. In tab. III, we exhibit the similarity among the ground truth and the RSS and phase signals with or without CPIX. We find that the raw data can hardly reflect human activity, especially the RSS profile. While CPIX can significantly improve the similarity even in multipath-prevalent environments. So CPIX can accurately retrieve the human movement trajectory in different environments, which may improve the accuracy and practicability of the human activity sensing system.

Apply CPIX in state-of-the-art sensing system. We also apply CPIX to a state-of-the-art human behavior sensing work, RFIPad [7], and evaluate its performance. RFIPad is a human hand gesture detection system, which can recognize touch-pad actions and 26 English letters by detecting every stroke people "write" in the air. As shown in Fig. 12, we form 25 tags in a 5×5 array, with an equal interval of 6cm. People can perform in-air handwriting on the virtual screen. We employ the same experiment deployment in the RFIPad work: a directional antenna placing face the tag array with a people in-between. In fact, some of the English letters are similar to
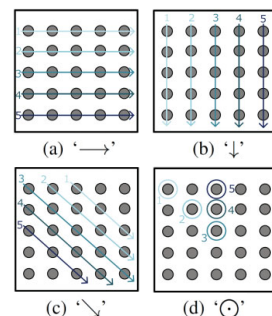
each other, *e.g.*, 'H' and 'A', 'X' and 'V', 'P' and 'D', *etc.*. As a result, detecting every stroke accurately is necessary for letter recognition. We choose four kinds of typical strokes, namely '⟶', '↓', '↘', '⊙ (click)'. As shown in Fig. 13, for every stroke, we choose five possible hand trajectories (or positions). We repeat each hand trajectory for 10 times and determine which gesture the person performs. To observe the influences of multipath effects on system performance, we place the system in a crowded office room. We employ the same recognition algorithm proposed in RFIPad and feed it with the data with or without CPIX. Note that RFIPad may use either the phase or RSS data. Hence we compare the recognition accuracy of both directly measured data (w/o CPIX) and CPIX data (with CPIX) when utilizing phase or RSS. The recognition accuracy of RFIPad with/ without CPIX is exhibited in Table IV, which shows that employing CPIX can improve the recognition accuracy significantly. In most situations, CPIX can improve the accuracy to around 90% compared to the original accuracy (70%-80%).

VI. CONCLUSION

In this paper, we present CPIX, the first generalized and low-cost solution to calculate accurate clean physical information for RFID sensing in the practical multipath-prevent environment. We use a new signal analysis model to extract the clean physical information using multi-channel measurement. We study two use cases of CPIX: tag localization and human behaviour sensing. The experiments indict that CPIX can achieve good accuracies.

REFERENCES

[1] ADIB, F., KABELAC, Z., AND KATABI, D. Multi-person localization via RF body reflections. In *Proceedings of USENIX NSDI* (2015).

[2] AZZOUZI, S., CREMER, M., DETTMAR, U., KRONBERGER, R., AND KNIE, T. New measurement results for the localization of UHF RFID transponders using an angle of arrival (AOA) approach. In *Proceedings of IEEE RFID* (2011).

[3] BOUET, M., AND DOS SANTOS, A. L. RFID tags: Positioning principles and localization techniques. In *Proceedings of IEEE IFIP Wireless Days* (2008), pp. 1–5.

[4] CAI, H., WANG, G., SHI, X., XIE, J., WANG, M., AND QIAN, C. When tags 'read'each other: Enabling low-cost and convenient tag mutual identification. In *Proceedings of IEEE ICNP* (2019), IEEE.

[5] CHUO, L.-X., LUO, Z., SYLVESTER, D., BLAAUW, D., AND KIM, H.-S. Rf-echo: A non-line-of-sight indoor localization system using a low-power active rf reflector asic tag. In *Proceedings of ACM MobiCom* (2017).

[6] DING, H., QIAN, C., HAN, J., WANG, G., JIANG, Z., ZHAO, J., AND XI, W. Device-free Detection of Approach and Departure Behaviors using Backscatter Communication. In *Proceedings of ACM UbiComp* (2016).

[7] DING, H., QIAN, C., HAN, J., WANG, G., XI, W., ZHAO, K., AND ZHAO, J. RFIPad: Enabling Cost-efficient and Device-free In-air Handwriting using Passive Tags. In *Proceedings of IEEE ICDCS* (2017).

[8] DING, H., SHANGGUAN, L., YANG, Z., HAN, J., ZHOU, Z., YANG, P., XI, W., AND ZHAO, J. FEMO: A platform for free-weight exercise monitoring with RFIDs. In *Proceedings of ACM SenSys* (2015).

[9] EPCGLOBAL. EPC^{TM} radio-frequency identity protocols class-1 generation-2 UHF RFID protocol for communications at 860 MHz–960 MHz, 2005.

[10] EPCGLOBAL. Low level reader protocol(LLRP), 2010.

[11] ISLAM, S. K., AND HAIDER, M. R. *Sensors and low power signal processing*. Springer Science & Business Media, 2009.

[12] JIANG, W., MIAO, C., MA, F., YAO, S., WANG, Y., YUAN, Y., XUE, H., SONG, C., MA, X., KOUTSONIKOLAS, D., XU, W., AND SU, L. Towards Environment Independent Device Free Human Activity Recognition. In *Proceedings of ACM MobiCom* (2018).

[13] JIN, H., WANG, J., YANG, Z., KUMAR, S., AND HONG, J. WiSh: Towards a Wireless Shape-aware World Using Passive RFIDs. In *Proceedings of ACM MobiSys* (2018).

[14] JIN, H., YANG, Z., KUMAR, S., AND HONG, J. I. Towards Wearable Everyday Body-Frame Tracking Using Passive RFIDs. *Proceedings of ACM Interact of Mobile Wearable Ubiquitous Technology 1*, 4 (2018).

[15] KLOZAR, L., AND PROKOPEC, J. Propagation path loss models for mobile communication. In *Proceedings of IEEE International Conference Radioelektronika* (2011), pp. 1–4.

[16] LI, H., ZHANG, P., AL MOUBAYED, S., PATEL, S. N., AND SAMPLE, A. P. ID-Match: A Hybrid Computer Vision and RFID System for Recognizing Individuals in Groups. In *Proceedings of ACM CHI* (2016).

[17] LI, X., WANG, M., SHI, S., AND QIAN, C. VERID: towards verifiable IoT data management. In *Proceedings of ACM/IEEE IoTDI* (2019), pp. 118–129.

[18] LI, X., WANG, M., WANG, H., YU, Y., AND QIAN, C. Toward Secure and Efficient Communication for the Internet of Things. *IEEE/ACM Transactions on Networking* (2019), 1–14.

[19] LIN, Q., YANG, L., JIA, H., DUAN, C., AND LIU, Y. Revisiting Reading Rate with Mobility: Rate-Adaptive Reading in COTS RFID Systems. In *Proceedings of ACM CoNEXT* (2017).

[20] LIU, J., CHEN, M., CHEN, S., PAN, Q., AND JUN CHEN, L. Tag-Compass: Determining the Spatial Direction of an Object with Small Dimensions . In *Proceedings of IEEE INFOCOM* (2017).

[21] LIU, T., YANG, L., LIN, Q., GUO, Y., AND LIU, Y. Anchor-free backscatter positioning for RFID tags with high accuracy. In *Proceedings of IEEE INFOCOM* (2014).

[22] LOCKWOOD, E. H. Revision course in school mathematics. by parr h.e. . pp. viii, 206. 97p. (bell.). *Mathematical Gazette 56*, 397, viii–242.

[23] LUO, Z., ZHANG, Q., MA, Y., SINGH, M., AND ADIB, F. 3D backscatter localization for fine-grained robotics. In *Proceedings of USENIX NS* (2019).

[25] MA, Y., SELBY, N., AND ADIB, F. Drone Relays for Battery-Free Networks. In *Proceedings of ACM SIGCOMM* (2017).

[24] MA, Y., HUI, X., AND KAN, E. C. 3D Real-time Indoor Localization via Broadband Nonlinear Backscatter in Passive Devices with Centimeter Precision . In *Proceedings of ACM Mobicom* (2016).

[26] MA, Y., SELBY, N., AND ADIB, F. Minding the billions: Ultra-wideband localization for deployed rfid tags. In *Proceedings of ACM MobiCom* (2017).

[27] MIESEN, R., KIRSCH, F., AND VOSSIEK, M. Holographic localization of passive UHF RFID transponders. In *Proceedings of IEEE RFID* (2011).

[28] PARR, A., MIESEN, R., AND VOSSIEK, M. Inverse sar approach for localization of moving RFID tags. In *Proceedings of IEEE RFID* (2013).

[29] PRADHAN, S., CHAI, E., SUNDARESAN, K., QIU, L., KHOJASTEPOUR, M. A., AND RANGARAJAN, S. RIO: A Pervasive RFID-based Touch Gesture Interface. In *Proceedings of ACM Mobicom* (2017).

[30] SCHMIDT, R. Multiple emitter location and signal parameter estimation. *IEEE Transactions on antennas and propagation 34*, 3 (1986), 276–280.

[31] SHANGGUAN, L., AND JAMIESON, K. The design and implementation of a mobile RFID tag sorting robot. In *Proceedings of ACM MobiSys* (2016).

[32] SHANGGUAN, L., LI, Z., YANG, Z., LI, M., AND LIU, Y. OTrack: Order tracking for luggage in mobile RFID systems. In *Proceedings of IEEE INFOCOM* (2013).

[33] SHANGGUAN, L., YANG, Z., LIU, A. X., ZHOU, Z., AND LIU, Y. Relative localization of RFID tags using spatial-temporal phase profiling. In *Proceedings of USENIX NSDI* (2015).

[34] SHANGGUAN, L., ZHOU, Z., AND JAMIESON, K. Enabling Gesture-based Interactions with Objects. In *Proceedings of ACM MobiSys* (2017).

[35] SHANGGUAN, L., ZHOU, Z., ZHENG, X., YANG, L., LIU, Y., AND HAN, J. Shopminer: Mining customer shopping behavior in physical clothing stores with COTS RFID devices. In *Proceedings of ACM SenSys* (2015).

[36] SHI, X., WANG, M., WANG, G., HUANG, B., CAI, H., XIE, J., AND QIAN, C. TagAttention: Mobile Object Tracing without Object Appearance Information by Vision-RFID Fusion. In *Proceedings of IEEE ICNP* (2019).

[37] VASISHT, D., KUMAR, S., AND KATABI, D. Decimeter-level localization with a single WiFi access point. In *Proceedings of USENIX NSDI* (2016).

[38] VASISHT, D., ZHANG, G., ABARI, O., LU, H.-M., FLANZ, J., AND KATABI, D. In-body backscatter communication and localization. In *Proceedings of ACM SIGCOMM* (2018).

[39] WANG, G., QIAN, C., CUI, K., DING, H., XI, W., HAN, J., AND ZHAO, J. A (Near) Zero-cost and Universal Method to Combat Multipaths for RFID Sensing. In *Proceedings of IEEE ICNP* (2019), IEEE.

[40] WANG, G., QIAN, C., SHANGGUAN, L., DING, H., HAN, J., YANG, N., XI, W., AND ZHAO, J. Hmrl: Relative localization of rfid tags with static devices. In *Proceedings of IEEE SECON* (2017).

[41] WANG, J., ADIB, F., KNEPPER, R., KATABI, D., AND RUS, D. RF-compass: Robot object manipulation using RFIDs. In *Proceedings of ACM MobiCom* (2013).

[42] WANG, J., AND KATABI, D. Dude, where's my card?: RFID positioning that works with multipath and non-line of sight. In *Proceedings of ACM SIGCOMM* (2013).

[43] WANG, J., VASISHT, D., AND KATABI, D. RF-IDraw: Virtual touch screen in the air using RF signals. In *Proceedings of ACM SIGCOMM* (2014).

[44] WANG, W., LIU, A. X., AND SUN, K. Device-free gesture tracking using acoustic signals. In *Proceedings of ACM MOBICOM* (2016).

[45] WEI, T., AND ZHANG, X. Gyro in the Air: Tracking 3D Orientation of Batteryless Internet-of-Things. In *Proceedings of ACM Mobicom* (2016).

[46] YANG, L., CHEN, Y., LI, X., XIAO, C., LI, M., AND LIU, Y. Tagoram: Real-time tracking of mobile RFID tags to high precision using COTS devices. In *Proceedings of ACM MOBICOM* (2014).

[47] YANG, L., LIN, Q., LI, X., LIU, T., AND LIU, Y. See through walls with COTS RFID system! In *Proceedings of ACM MOBICOM* (2015).

[48] YANG, L., QI, Y., FANG, J., DING, X., LIU, T., AND LI, M. Frogeye: Perception of the slightest tag motion. In *Proceedings of IEEE INFOCOM* (2014).

[49] ZHAO, Y., LIU, Y., AND NI, L. M. VIRE: Active RFID-based localization using virtual reference elimination. In *Proceedings of IEEE ICPP* (2007).

[50] ZHOU, J., ZHANG, H., AND MO, L. Two-dimension localization of passive RFID tags using AOA estimation. In *Proceedings of IEEE I2MTC* (2011).